npg

ORIGINAL ARTICLE

Intracerebroventricular delivery of self-complementary adeno-associated virus serotype 9 to the adult rat brain

A Donsante[1], Z McEachin[1], J Riley[1], CH Leung[2], L Kanz[2], DM O'Connor[1] and NM Boulis[1]

Gene therapy for the central nervous system is poised to become a powerful treatment for numerous neurological disorders. Adeno-associated viral vectors based on serotype 9 (AAV9) have proven themselves to be strong candidates for delivering gene-based therapies throughout the brain and spinal cord when administered intravenously, intrathecally, intracisternally, and intracerebroventricularly (i.c.v.). Previous studies of i.c.v.-delivered self-complimentary AAV9 have been performed in neonatal mice with delivery of a single dose. However, before clinical trials can be considered, more information is required about the dose–response relationship for transduction efficiency in adult animals. In the current study, three doses of self-complementary AAV9 were administered to adult rats. High levels of transduction were observed in the hippocampus, cerebellum and cerebral cortex, and transduction increased with increasing dosage. Both neurons and astrocytes were transduced. There was no evidence of astrocytosis at the doses tested. Preliminary results from pigs receiving i.c.v. self-complementary AAV9 are also presented. The results of this study will serve to inform dosing studies in large animal models before clinical testing.

INTRODUCTION

Gene therapy has long been studied to treat diseases of the central nervous system (CNS). A wide variety of inherited metabolic diseases, such as lysosomal storage diseases, affect the brain, causing mental retardation and neurodegeneration. CNS disorders substantially affect the quality of life of patients and their family members, leading to loss of independence and difficulties in communication. Direct delivery of therapeutic genes to the brain offers a potent treatment for these diseases that circumvents problems found with systemic therapies. For example, neutralizing antibodies in the CNS are less of a concern,[1] and the risk of an immune response to the vector and/or the transgene seems to be lower,[2] although this risk is still not zero.[3]

For treating disorders that affect cells throughout the CNS, such as lysosomal storage diseases, one challenge for gene therapy is to achieve adequate transduction throughout the brain and spinal cord. As all cells in the CNS make contact with the cerebrospinal fluid (CSF), delivery of viral vectors to the CSF (intrathecally, intracisternally or intraventricularly) has been widely investigated. Larger volumes of vector can be safely delivered via CSF injection as compared with parenchymal injections. In addition, relative to intravenous delivery, off-target effects are also less likely. One vector in particular, adeno-associated virus serotype 9 (AAV9), has the ability to transduce many regions of the CNS following CSF delivery.[4]

A number of studies have examined intracerebroventricular (i.c.v.) delivery of AAV9. However, these studies examined treatments delivered during the neonatal or juvenile period.[5–8] As the brain is not fully developed during these periods, it is not clear how well these results might translate to adult animals. Indeed, Chakrabarty et al. have shown remarkable differences in transduction patterns when the treatment age was varied by a mere 1 to 2 days.[9] In addition, the small size and resilience of the neonatal mouse

allows for the delivery of large doses that may not be practical in a clinical setting. For instance, one mouse study administered a dose of $\sim 3 \times 10^{14}$ vector genomes (vg) per kg.[10] This dose is more than 100 times greater than that used in a recent clinical trial for hemophilia that was administered intravenously.[11]

With the exception of one canine study,[12] little is known about the biodistribution of AAV9 following i.c.v. injection into animals larger than mice. In addition, distribution of i.c.v. self-complimentary AAV9 (scAAV9), which is expected to yield better transduction than the traditional single-stranded AAV9 (ssAAV9), has not been examined outside of neonatal mouse studies. To better understand how scAAV9 will perform in the adult brain, we examined the dose–response relationship for i.c.v.-delivered scAAV9 into the adult rat using doses in the range expected to be used clinically in a human trial. This study will serve as the foundation for an ongoing comparative study in a large animal model, the farm pig. Together, these studies will inform future dosing decisions for human clinical trials of i.c.v. scAAV9.

RESULTS

Transduction biodistribution

To determine what doses might be used clinically, two main limiting factors were considered: viral titer and the volume that can safely be delivered in a reasonable amount of time. Viral titers of clinical grade vector generally range from 10^{13} to 10^{14} vg ml^{-1}. We estimate that 5–10% of the CSF volume can be delivered in a single bolus i.c.v. injection, corresponding to ~ 8–16 ml in an adult. Based on these estimates, the maximum adult i.c.v. dose would be $\sim 10^{15}$ vg. Scaling the dose down based on the rat CSF volume, this dose corresponds to $\sim 3 \times 10^{12}$ vg in an adult rat. As this dose

[1]Department of Neurosurgery, Emory University School of Medicine, Atlanta, GA, USA and [2]Department of Biology, Widener University, Chester, PA, USA. Correspondence: Dr NM Boulis, Department of Neurosurgery, Emory University School of Medicine, 1365B Clifton Road NE, Suite B6200, Atlanta, GA 30322, USA.
E-mail: nboulis@emory.edu

represents the maximum under ideal conditions, the highest dose tested in this study was one-third of this maximum.

Adult Sprague-Dawley rats received a unilateral injection of scAAV9-GFP into the lateral ventricle and were killed 3 weeks later. Three doses were evaluated: 3.1 µl (low dose, 3.7×10^{10} vg), 15.5 µl (medium dose, 1.9×10^{11} vg) and 77.5 µl (high dose, 9.3×10^{11} vg). In addition, a fourth cohort was included that used the lowest dose of virus (3.7×10^{10} vg) delivered at the highest volume (77.5 µl) to account for differences in delivery volume (low dose/ high volume). Representative images of the brains of high-dose-treated rats stained for green fluorescent protein (GFP) are presented in Figure 1. Two types of distribution were apparent at low magnification. In the cerebral cortex and cerebellum, the cells were evenly distributed across these regions. Qualitative analysis revealed similar GFP expression in the injected and uninjected hemispheres, with the exception of the area adjacent to the injection track that showed a high degree of GFP expression. In contrast, limbic regions, such as the hippocampus and the striatum, exhibited different transduction patterns between the two sides of the brain following unilateral injection into the lateral ventricle. Sections of cervical spinal cord stained positively for GFP, particularly in the high-dose group (Figure 1c). However, there was little evidence of transduction of cell bodies in the ventral gray matter. Instead, most of the staining appeared to be axonal projections from neurons that lie outside of the spinal cord.

Both neuronal and glial cells were transduced with i.c.v. delivery. As the vector was delivered to the lateral ventricles, we first looked for transduction in the choroid plexus and the ependymal cell layer. There were many GFP$^+$ cells in both structures (Figure 2a). Neurons were also transduced. Staining for GFP and NeuN, a neuronal nuclei marker, colabeled cells in both the cerebral cortex and the granular layers of the hippocampus (Figure 2b). Although neurons were transduced throughout the cerebral cortex, GAD67-expressing GABAergic neurons were not transduced (Figure 2f). In the cerebellum, Fox2, a nuclei marker

that labels Purkinje cells, colocalized with GFP staining, indicating transduction of this cell type (Figure 2c). These GFP$^+$ cells also stained positively for calbindin that is expressed by several types of neurons, including Purkinje cells (Figure 2d).[13] Many cells with an astrocytic morphology were transduced. However, no colocalization of glial fibrillary acidic protein (GFAP) and GFP was observed (Figure 2e), except in close proximity to the injection track. However, S100β, another marker for astrocytes, did colocalize with these GFP$^+$ cells, indicating astrocyte transduction (Figure 2g).

### Transduction efficiency in the brain

The GFP$^+$ area was measured in three brain regions: cerebral cortex, hippocampus and cerebellum (Figure 3). Increasing scAAV9 dose generally led to increased transduction in all three brain regions. In the hippocampus, 25 to 35% of the area was GFP$^+$, much of the staining occurring outside of the granular layers. In the cerebellum, GFP$^+$ cells accounted for 5 to 32% of the area of the molecular layer, predominantly from the transduction of Purkinje neurons. The cerebral cortex had the lowest level of transduction of the three regions quantified, with 1 to 10% of the area GFP$^+$.
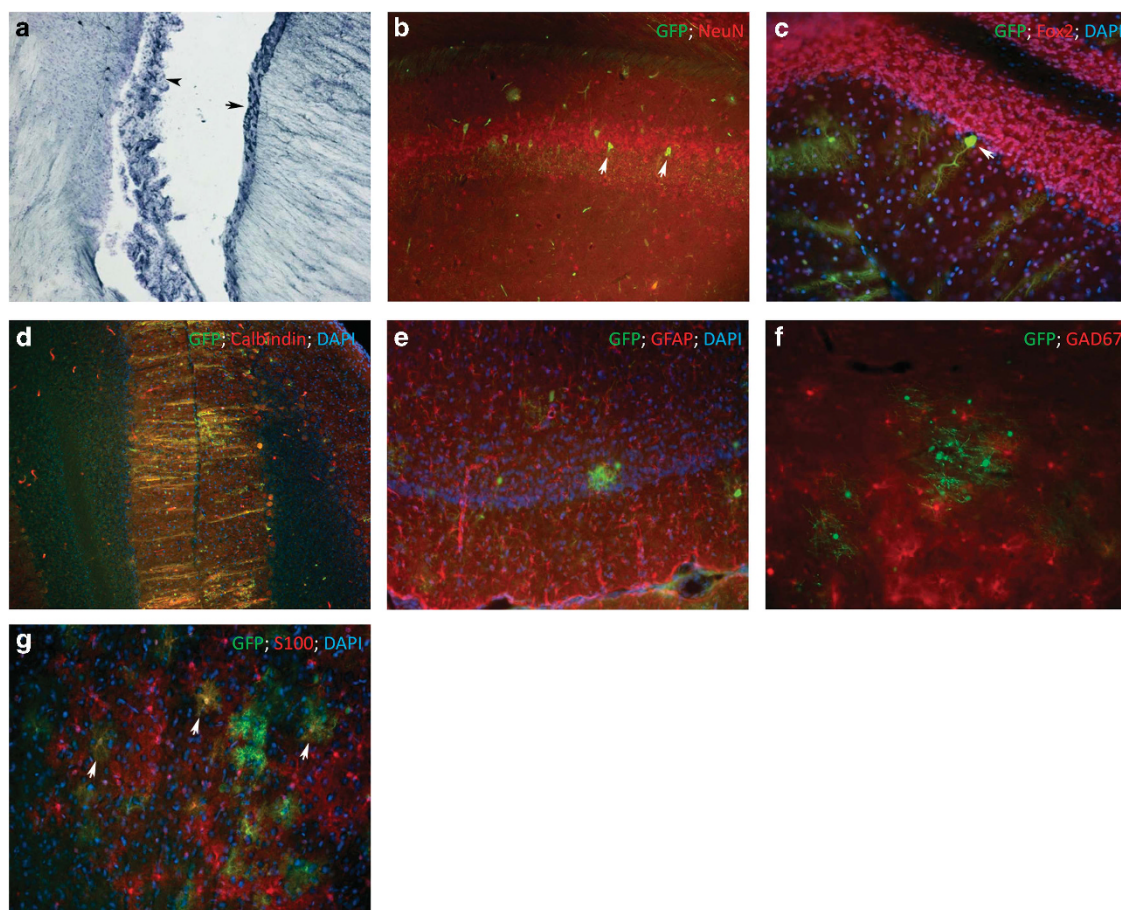
Non-CNS transduction

To determine whether scAAV9 escaped to the periphery following i.c.v. injection, liver samples were stained for GFP. Very few GFP cells were identified (data not shown, one positive cell in 18 cm^2 of tissue evaluated from medium-dose rats), suggesting that the amount of scAAV9 that escaped from the CNS was small.

Astrocyte activation

The introduction of foreign viruses and proteins can elicit an immune response in the CNS, often presenting as astrogliosis.
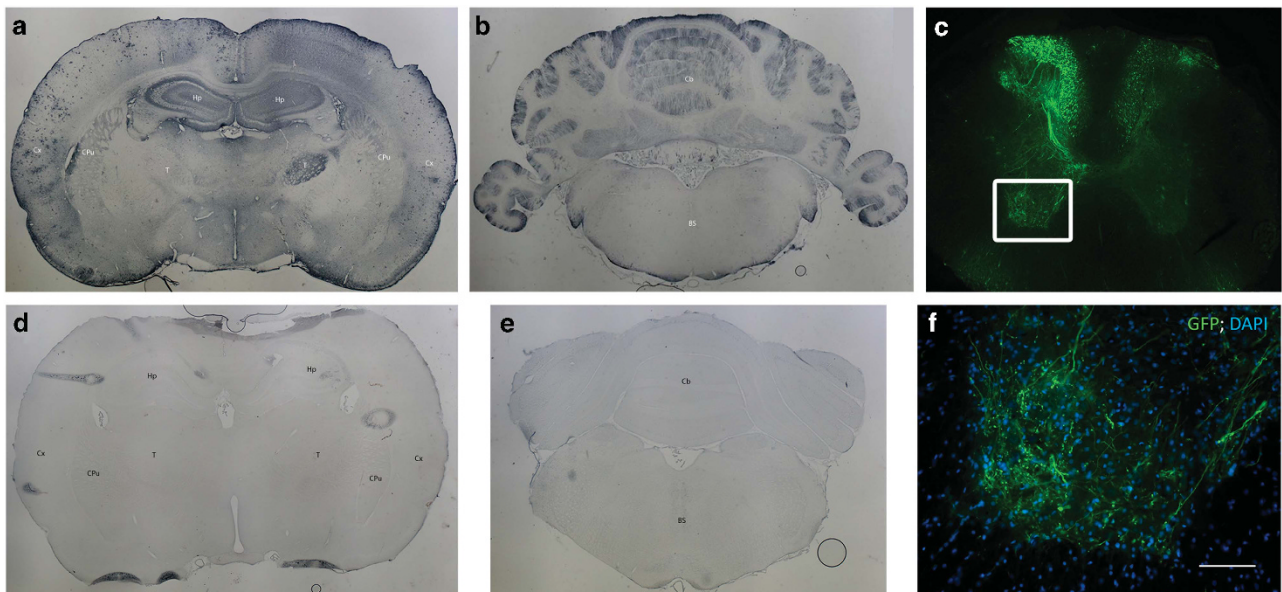
Figure 1. Widespread transduction of the CNS occurs following i.c.v. scAAV9 delivery. Sprague-Dawley rats were killed 3 weeks after receiving i.c.v. injection of scAAV9-GFP or saline. (**a**, **b**, **d**, **e**) Brain and spinal cord sections were stained for GFP (black stain). Sections from a high-dose rats are shown at (**a**) ~2.1 mm and (**b**) ~11.3 mm caudal of Bregma. Comparable regions from a saline-treated rats are shown, revealing limited background staining (**d**, **e**). Notably, there was substantial transduction of the (**a**) cerebral cortex, hippocampus and (**b**) cerebellum. Transduction was also high on the right side of the brain in the proximity of the injection tract. Deeper brain structures showed less transduction. (**c**) Transduction of the spinal cord was evaluated by immunofluorescence (green stain). A ventral horn, boxed in (**c**), is shown magnified in (**f**). In contrast to the brain, there was little staining of cell bodies in the gray matter. Instead, the majority of the GFP staining appeared to be axons. (**f**) Scale bar, 100 µm. BS, brain stem; Cb, cerebellum; Cpu, caudate putamen; Cx, cerebral cortex; Hp, hippocampus; T, thalamus.

Figure 2. The scAAV9 transduces several cell types when delivered by i.c.v. injection in the rat. (**a**) Brain sections from scAAV9-GFP-treated rats stained for GFP (black) demonstrate significant transduction of the choroid plexus (arrowhead) and ependyma (arrow), particularly in the injected ventricle. (**b–g**) Brain sections were costained for GFP (green) and cell markers (red): (**b**) NeuN, (**c**) Fox2, (**d**) calbindin, (**e**) GFAP, (**f**) GAD67 and (**g**) S100β. Colocalization of between GFP and cell markers is indicated by arrows. (**b**) A representative image from a high-dose animal shows colocalization of NeuN and GFP in hippocampal neurons. Colocalization with NeuN was also observed in the cerebral cortex (data not shown). (**c**) The cerebellum of a low-dose animal is shown. Purkinje cells, identified by their elaborate dendritic tree and the presence of Fox2 in the nucleus, are the primary cell transduced. (**d**) Staining for calbindin, which stains a variety of neurons including Purkinje cells, also showed extensive colocalization with GFP (orange to yellow), supporting the conclusion that the majority of GFP expression in the cerebellum is due to Purkinje cell transduction. GFP⁺ cells with morphology reminiscent of astrocytes were observed regularly in the cerebral cortex. Staining for (**d**) GFAP, a marker for astrocytes, and (**e**) GAD67, a marker for interneurons, failed to show colocalization with GFP for these cells. (**f**) However, S100β, a marker for a subset of astrocytes, stained most, if not all, of the cells with this morphology.

To look for the presence of activated astrocytes, we stained brain sections from two phosphate-buffered saline-treated and two high-dose scAAV9-treated rats for GFAP. Eight sections, taken from regions adjacent to those illustrated in Figure 1, were evaluated per animal, four from the cerebellum and four that included the hippocampus and cerebral cortex. GFAP staining was evaluated at low magnification to look for global changes in astrocyte activation and at higher magnification in the cerebellum, hippocampus and cerebral cortex to look for local changes. No discernible change in staining was observed in the AAV-treated animals relative to the saline-treated animals.

Intracerebroventricular I.C.V. injection into the adult pig

Three adult farm pigs received a unilateral injection of scAAV9-GFP, with doses ranging from 2.01×10^{13} to 6.03×10^{13} vg in volumes from 1.5 to 4.5 ml. After 3 weeks, the animals were killed. Results were similar from all three pigs. Representative sections are shown in Figure 4. Like the rat, there is substantial transduction of the cerebral cortex, hippocampus and cerebellum. Morphologically, these cells appear similar in appearance to those

found in the rat, suggesting transduction of both neurons, including Purkinje cells, and astrocytes.

DISCUSSION

We have presented a dose-escalation study of i.c.v. scAAV9-GFP in rats to examine the biodistribution of the vector using a range of doses expected in future clinical trials, and we have begun to extend our observations to a large animal model. Unilateral i.c.v. injection of scAAV9-GFP led to even transduction across the entire cerebral cortex and cerebellum, whereas a substantial variation between the two hemispheres was observed in deeper structures, such as the hippocampus (Figure 1). The cause of this dichotomy is not immediately obvious. One possible hypothesis for this finding is that the majority of virus reaching the cerebellum and cerebral cortex does so by traveling through the ventricular system to the subarachnoid space and then into the tissue, whereas deeper structures are transduced by vector passing through the ependymal layer, perhaps through the needle track. Whatever the source of this variation, these results suggest that bilateral i.c.v. injection may be preferable in a clinical setting.
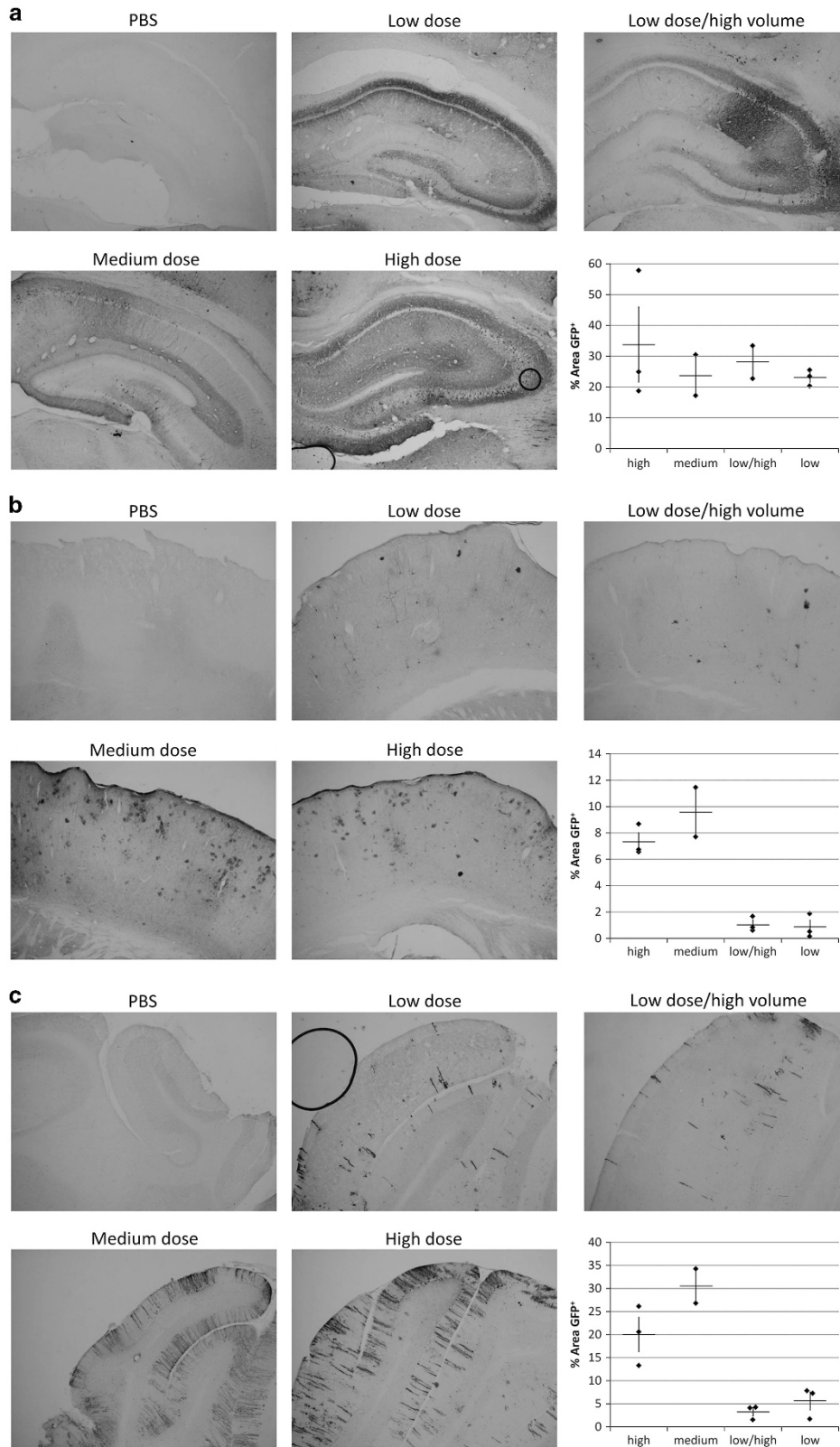
Figure 3. The scAAV9 transduction distribution. Transduction was quantified in three brain regions ((**a**) hippocampus, (**b**) cerebral cortex and (**c**) cerebellum) in five treatment groups (phosphate-buffered saline (PBS) controls, low dose, low dose/high volume, medium dose and high dose). Each group consisted of three animals, except for the medium dose that had two. Individual animals are plotted on the graphs. The horizontal bars represent the average for each group and the error bars indicate the s.e.m. There was a general trend toward greater transduction with increasing dose. Increasing the injection volume did not seem to play a major role in the distribution of transduction. For the cerebral cortex and cerebellum, the medium- and high-dose groups were significantly different than the low-dose and low-dose/high-volume groups ($P < 0.05$).
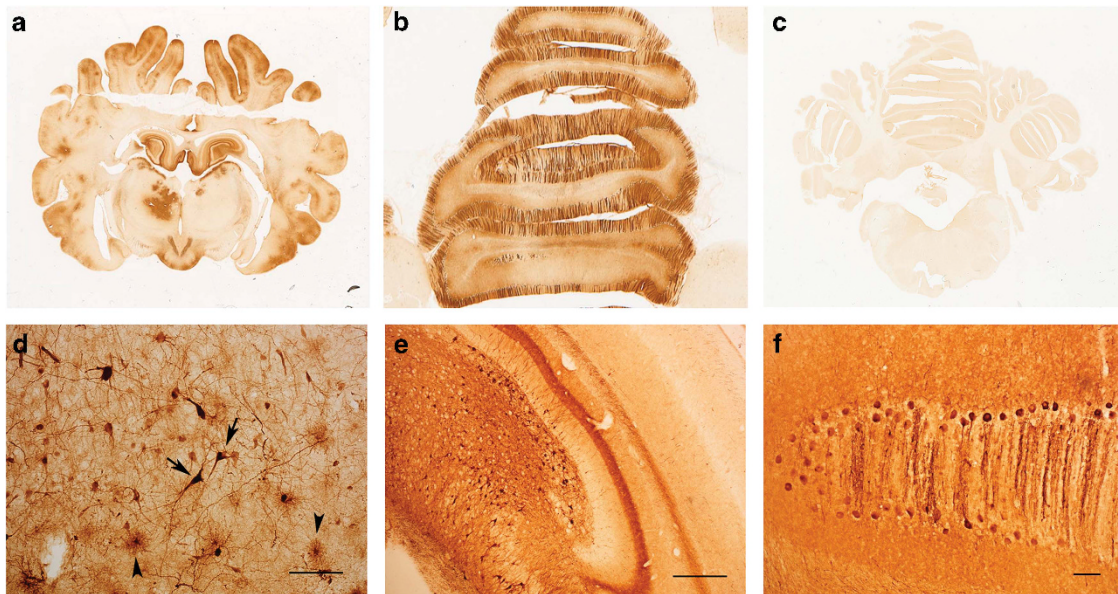
Figure 4. The scAAV9 transduction in the pig. At 3 weeks following i.c.v. injection of scAAV9-GFP into one lateral ventricle, the brain was harvested, sectioned and stained for GFP (brown stain). Consistent with the observations in the rats, substantial transduction was observed in the (**a**) hippocampus, cerebral cortex and (**b**) cerebellum. The brain of an untreated pig shows no staining for GFP (**c**). Photomicrographs taken at higher magnification are shown for (**d**) cerebral cortex, (**e**) hippocampus and (**f**) cerebellum. In (**d**), arrows indicate examples of cells with neuronal morphology. Arrowheads indicate examples of cells exhibiting the morphology of astrocytes. The pattern of neuronal and glial transduction, based on morphology, is similar to what was seen in the rat. Scale bars, 100 μm (**d**, **f**) and 500 μm (**e**).

The i.c.v. scAAV9-GFP injections into the pig mimic the transduction pattern that we have observed in the rat (Figures 1 and 4). These preliminary data suggest that the transduction pattern observed in the rat will extend into larger mammalian brains.

The i.c.v. delivery of ssAAV9 vectors has been reported in both mice and dogs. There are two notable differences between the transduction patterns observed in these species when compared with our study. In mice treated at P21, the transduction profile is a primarily neuronal in nature, although there is little transduction of Purkinje neurons. Astrocytes are poorly transduced.[7] In i.c.v.-ssAAV9-treated adult dogs, the same pattern of transduction is found.[12] In contrast, our i.c.v.-scAAV9-treated rats and pigs have substantial transduction of astrocytes as well as neurons, and there is substantial transduction of cells in the cerebellum, particularly of Purkinje neurons. Thus, the cellular tropism and distribution pattern in this study differ markedly from previously published i.c.v. studies in other species.

To our knowledge, i.c.v. delivery of AAV9, either scAAV9 or ssAAV9, has not yet been conducted in primates. However, cisterna magna delivery of scAAV9-GFP has been evaluated in macaques.[14] The authors of this study reported colocalization of GFP with neuronal and astrocytic markers, and the overall pattern of transduction in the cerebral cortex and cerebellum appears similar to what we have observed in rats and pigs. One notable difference between this macaque study and our current study is that the primates also exhibit transduction of GFAP[+] astrocytes in addition to S100β[+] astrocytes, whereas our rodent study mainly found transduction of S100β[+] astrocytes throughout the brain, with GFP colocalizing with GFAP only around the injection tract.

It is unclear what the implications of this difference are. Differences in AAV transduction can arise from differences in dose, method of delivery, age and species. In recent years it has become clear that astrocytes are not a monolithic collection of cells. GFAP, generally used as a marker of astrocytes, is not immunohistochemically detectable in a subpopulation of these cell.[15] In addition, different subpopulations of astrocytes respond to stimuli in different ways,[16] and the variety of subtypes of astrocytes can vary across species.[17] One hypothesis that could explain the differences between primate and rat astrocytes transduction could be a preference of AAV9 for a particular subpopulation of astrocytes in the rat (a subset labeled with S100β). Alternatively, it is possible that the GFAP[+] astrocytes transduced in the primate are not present in rats.

Given their evolutionary lineages, it is unexpected that rats, pigs and primates would exhibit one transduction pattern (a mixture of neuronal and astrocytic transduction, high levels of cerebellar transduction) for AAV9, whereas mice and dogs would have another (neuronal transduction, poor cerebellar transduction). These divergent results led us to search for possible explanations. In examining the previous studies more closely, we identified one variable that correlated with the transduction pattern. Our study and the primate study[14] utilized scAAV9, whereas the mouse study[7] and the dog study[12] employed ssAAV9. It has been well documented that scAAV vectors outperform ssAAV vectors by bypassing the need for second-strand synthesis.[18–22] This leads to increased numbers of cells being transduced, faster transgene expression and higher levels of transgene produced. However, to the best of our knowledge, there have been no previous reports of ssAAV and scAAV vectors of the same serotype exhibiting different cellular tropisms. If this first-of-its-kind observation can be corroborated, it will have important implications for the field. The differences observed above suggest that Purkinje neurons and astrocytes are less amenable to targeting by ssAAV9 vectors when compared with scAAV9 vectors. If so, this could represent a potential barrier for therapies using ssAAV to target these cell types. One explanation for this difference could be that these cell types exhibit substantially lower efficiencies for second-strand synthesis relative to cortical neurons, reducing the probability that a ssAAV vector will reach a transcriptionally active state. This could point to differences in DNA repair pathways between these cell types that might contribute to Purkinje cells being more susceptible to degeneration in certain diseases.

The delivery of a foreign protein, be it simply a marker or a therapeutic gene (in the case of individuals with two null mutations), carries with it the risk of an adaptive immune response against the protein that can, in turn, cause loss of

transduced cells. Astrocytes, in particular, can serve as antigen-presenting cells.[23] Therefore, the transduction of S100β$^+$ astrocytes seen after scAAV9 delivery may be of concern. Indeed, Samaranch et al.[24] observed behavioral defects in primates 3 weeks after intrathecal delivery of AAV9 that correlated with loss of Purkinje neurons. Interestingly, this loss was transgene dependent. Expression of a foreign protein, GFP, led to behavioral abnormalities, whereas expression of a self-recognized protein, hAADC, had little or no adverse effects.[24] We did not observe any overt behavioral changes in our rats, and staining for GFAP did not reveal signs of astrogliosis. However, the highest dose that we used was somewhat lower than the dose used in the primate study by Samaranch et al.[24] The delivery method was also different (i.c.v. vs cisterna magna), although both studies investigated delivery of virus to the CSF. Longer follow-up may be warranted to look for inflammation at later time points and for the loss of transduced cells. Immunosuppression may be required in the clinical setting.[3]

A number of disorders will be good candidates for i.c.v. AAV9-mediated therapies. Lysosomal storage diseases are one example. Most of these disorders are because of deficiencies in a single acid hydrolase.[25] Although these enzymes are essentially needed in every cell, they can be secreted from transduced cells and taken up by nearby deficient cells in a process known as cross-correction.[26] The widespread transduction that we have observed would seem to be ideal for the treatment of this type of disorder. Indeed, i.c.v. AAV9 treatment of mucopolysaccharidosis IIIB mice led to substantial improvements in biochemical and histological measurements of disease as well as increased lifespan to normal or near-normal levels.[12] Given the high levels of Purkinje neuron transduction observed in our study, diseases affecting these cells, such as spinocerebellar ataxias, would also be obvious targets of i.c.v. scAAV9-mediated gene therapy. This delivery route would avoid direct injection into the parenchyma and would presumably be safer.[27,28]

MATERIALS AND METHODS

Vector

Self-complimentary AAV9 was generously donated to the lab by Dr Marco Passini (Genzyme, Boston, MA, USA). The expression vector uses a proprietary mini-chicken β-actin promoter to drive expression of an enhanced GFP complementary DNA. In the rat studies, the vector titer used was 1.2×10^{13} vg ml^{-1}. For the pig study, scAAV9 expressing GFP from a cytomegalovirus enhancer/chicken β-actin promoter was purchased from Nationwide Children's Hospital's vector core (Columbus, OH, USA). It was used at a concentration of 1.34×10^{13} vg ml^{-1}.

Animal surgery

All animal procedures were done with approval of the Emory University institutional animal care and use committee. Male Sprague-Dawley rats were obtained from Charles River Labs (catalog number 400, 276–300 g body weight; Wilmington, MA, USA) and allowed to acclimate to the animal facility for 2 to 7 days before surgery was performed. Rats were maintained on a 12:12 h light/dark cycle with food (Labdiet 5001; Labdiet, St Louis, MO, USA) and tap water provided ad libitum. Individual rats were randomly assigned to the treatment groups described below.

Rats were anesthetized and maintained on 2% isoflurane/98% oxygen throughout the procedure (0.6 l min^{-1}). The head was immobilized in a stereotactic frame using a nose cone and ear bars. The top of the head was shaved and sterilized with ethanol and betadine, and a sterile drape was applied around the surgical site. Lidocaine was administered subcutaneously, and buprinorphine (0.1 mg kg^{-1}) was administered to alleviate postoperative pain. Using a dental drill, a burr hole was drilled through the skull unilaterally at a position 0.8 mm posterior to Bregma and 1.6 mm lateral from midline. Vector was delivered using a Hamilton syringe with a 27-gauge needle affixed to a micromanipulator. Three doses were evaluated: 3.1 μl (low dose, 3.7×10^{10} vg; $n = 3$), 15.5 μl (medium dose, 1.9×10^{11} vg; $n = 2$) and 77.5 μl (high dose, 9.3×10^{11} vg; $n = 3$). In addition, a fourth cohort was included that used the lowest dose of virus

(3.7×10^{10} vg) delivered at the highest volume (77.5 μl) to account for differences in delivery volume (low dose/high volume; $n = 3$). Vector was injected at a rate of ~ 25 μl min^{-1}, controlled by a manual injection knob on the micromanipulator. The needle was left in place for 1 min following the injection and then slowly withdrawn. The skin was closed and the animal was kept warm during recovery. After 3 weeks, the animals were killed and perfused with saline followed by 4% paraformaldehyde. Brain, spinal cord and liver tissue were postfixed in 4% paraformaldehyde overnight followed by cryopreservation in sucrose. Tissue was frozen on dry ice and stored at − 80 °C before sectioning.

Farm pigs (30 kg) were obtained from Palmetto Research Swine (Reevesville, SC, USA). Animals were sedated with 0.8 mg kg^{-1} acepromazine, 33 mg kg^{-1} ketamine and 0.04 mg kg^{-1} atropine. Anesthesia was maintained using isoflurane. Pain was managed with a fetanyl patch (100 μg h^{-1} for 3 days). The skin was incised in a paramedian orientation and dissection was carried down to the occipital keel. A burr hole was drilled ~ 1 cm posterior and medial to the ipsilateral supraorbital foramen with a high-speed Midas Legend. The dura was punctured with an 18-gauge needle. A proximal ventriculoperitoneal shunt catheter was inserted ~ 2.5 cm into the brain at a posterior and slightly medial direction toward the ipsilateral frontal horn of the right lateral ventricle until it was felt penetrating the ventricle. Correct placement of the needle was determined by observing flow of CSF once the stylet was withdrawn. Placement was confirmed by contrast ventriculography using Omnipaque-300 radiocontrast dye (GE Healthcare, Little Chalfont, UK). The catheter was advanced an additional 1 cm, and 3 ml of CSF was removed. Then, 1.5 to 4.5 ml of AAV9-GFP (1.34×10^{13} vg ml^{-1} in 20 mM Tris, pH 8.0, 1 mM MgCl$_2$, 200 mM NaCl+0.001% Pluronic F68) were delivered over 10 min using a MINJ-PD pump (Tritech Research, Los Angeles, CA, USA). The catheter was left in place for an additional 15 min and then removed. A small piece of gelfoam was placed over the parenchymal penetration site and the burr hole was sealed with bone wax. The skin was closed with interrupted 3-0 vicryl suture followed by running 2-0 ethilon. After 22 days, the animals received intravenous heparin followed by perfusion with saline and 4% paraformaldehyde and the brains were harvested. Tissue was cryopreserved in 30% sucrose before sectioning.

Histology

Coronal sections (40 μm) were cut on a Leica CM1950 cryostat (Wetzlar, Germany). Primary antibodies for GFP (AB3080P, Millipore, Billerica, MA, USA), GFAP (MAB360, Millipore), NeuN (MAB377, Millipore), S100β (MAB079-1, Millipore), Fox-2 (ab167282, Abcam, Cambridge, MA, USA), Calbindin (C9848, Sigma, Saint Louis, MO, USA) and GAD67 (MAB5406, Millipore) were used at 1:500 dilution for immunohistochemistry. Antigen retrieval for S100β and Fox-2 was performed using citrate buffer (10 mM sodium citrate, pH 6.0) for 20 min at 52 or 95 °C, respectively. For fluorescent microscopy, an Alexa Fluor 488-conjugated goat anti-rabbit secondary (A11070, Life Technologies, Grand Island, NY, USA) was used to detect GFP and an Alexa Fluor 596-conjugated goat anti-mouse secondary (A11032, Life Technologies) was used to detect the cell type markers at a 1:500 dilution. For chromogenic detection of GFP$^+$ cells, a biotin-conjugated goat anti-rabbit secondary (111-065-144, Jackson Immunoresearch, West Grove, PA, USA) was used at a 1:250 dilution followed by a Vector ABC kit and HRP detection system (Vector, Burlingame, CA, USA). Slides were imaged with a Nikon (Tokyo, Japan) Eclipse E400 microscope with fluorescence filters (UV-2E/C, B-2E/C, and G-2E/C) and a Nikon Digital Sight controller with DS-Qi1Mc and DS-Fi1 cameras.

Transduction quantification

Using the 4× objective, JPEG images were taken of the hippocampus, cerebral cortex and cerebellum. The intensity of the light source and the exposure time were held constant. Images were imported into ImageJ (http://imagej.nih.gov/ij/) for analysis. Individuals performing the analysis were blinded to the four AAV treatment groups. For each image, the areas outside of the region of interest were first masked (not included in the analysis). For the hippocampus and cerebral cortex, brain regions adjacent to these areas were excluded from the analysis. For the cerebellum, regions of the image outside of the molecular layer were excluded. The three color channels (red, green and blue) were split into three separate 8-bit gray-scale images. Using the images from the green channel, the fraction of pixels in the image with values between 0 and a predetermined threshold were calculated. As the histochemical stain is black, pixels within this range of values should correspond to those that cover stained portions of the

section. Phosphate-buffered saline-treated controls were used to empirically set the threshold for each region to minimize the detection of background staining. Using the red channel, the fraction of pixels in the region of interest (that is, the pixels that were not masked) was similarly determined. Dividing the fraction of pixels that were stained positively by the fraction of pixels covering the region of interest and multiplying by 100 yielded the fraction of the region of interest that was GFP$^+$. For the cerebral cortex and hippocampus, four images were analyzed per animal taken evenly from the left and right sides of the brain to average out differences between the injected and uninjected sides. Similarly, six images of the cerebellum were analyzed for each animal (two right, two center and two left). Differences between treatment groups were determined by two-tailed t-test.

CONFLICT OF INTEREST

The authors declare no conflict of interest.

ACKNOWLEDGEMENTS

REFERENCES

1 Gray SJ, Nagabhushan Kalburgi S, McCown TJ, Jude Samulski R. Global CNS gene delivery and evasion of anti-AAV-neutralizing antibodies by intrathecal AAV administration in non-human primates. Gene Therapy 2013; 20: 450–459.

2 Mingozzi F, High KA. Immune responses to AAV vectors: overcoming barriers to successful gene therapy. Blood 2013; 122: 23–36.

3 Ellinwood NM, Ausseil J, Desmaris N, Bigou S, Liu S, Jens JK et al. Safe, efficient, and reproducible gene therapy of the brain in the dog models of Sanfilippo and Hurler syndromes. Mol Ther 2011; 19: 251–259.

4 Dayton RD, Wang DB, Klein RL. The advent of AAV9 expands applications for brain and spinal cord gene delivery. Expert Opin Biol Ther 2012; 12: 757–766.

5 McLean JR, Smith GA, Rocha EM, Hayes MA, Beagan JA, Hallett PJ et al. Widespread neuron-specific transgene expression in brain and spinal cord following synapsin promoter-driven AAV9 neonatal intracerebroventricular injection. Neurosci Lett 2014; 576: 73–78.

6 Levites Y, Jansen K, Smithson LA, Dakin R, Holloway VM, Das P et al. Intracranial adeno-associated virus-mediated delivery of anti-pan amyloid beta, amyloid beta40, and amyloid beta42 single-chain variable fragments attenuates plaque pathology in amyloid precursor protein mice. J Neurosci 2006; 26: 11923–11928.

7 Gholizadeh S, Tharmalingam S, Macaldaz ME, Hampson DR. Transduction of the central nervous system after intracerebroventricular injection of adeno-associated viral vectors in neonatal and juvenile mice. Hum Gene Ther Methods 2013; 24: 205–213.

8 Dirren E, Towne CL, Setola V, Redmond Jr DE, Schneider BL, Aebischer P. Intracerebroventricular injection of adeno-associated virus 6 and 9 vectors for cell type-specific transgene expression in the spinal cord. Hum Gene Ther 2014; 25: 109–120.

9 Chakrabarty P, Rosario A, Cruz P, Siemienski Z, Ceballos-Diaz C, Crosby K et al. Capsid serotype and timing of injection determines AAV transduction in the neonatal mice brain. PLoS One 2013; 8: e67680.

10 Broekman ML, Baek RC, Comer LA, Fernandez JL, Seyfried TN, Sena-Esteves M. Complete correction of enzymatic deficiency and neurochemistry in the GM1-gangliosidosis mouse brain by neonatal adeno-associated virus-mediated gene delivery. Mol Ther 2007; 15: 30–37.

11 Nathwani AC, Tuddenham EG, Rangarajan S, Rosales C, McIntosh J, Linch DC et al. Adenovirus-associated virus vector-mediated gene transfer in hemophilia B. N Engl J Med 2011; 365: 2357–2365.

12 Haurigot V, Marco S, Ribera A, Garcia M, Ruzo A, Villacampa P et al. Whole body correction of mucopolysaccharidosis IIIA by intracerebrospinal fluid gene therapy. J Clin Invest 2013; 123: 3254–3271.

13 Bastianelli E. Distribution of calcium-binding proteins in the cerebellum. Cerebellum 2003; 2: 242–262.

14 Samaranch L, Salegio EA, San Sebastian W, Kells AP, Foust KD, Bringas JR et al. Adeno-associated virus serotype 9 transduction in the central nervous system of nonhuman primates. Hum Gene Ther 2012; 23: 382–389.

15 Sofroniew MV, Vinters HV. Astrocytes: biology and pathology. Acta Neuropathol 2010; 119: 7–35.

16 Benesova J, Hock M, Butenko O, Prajerova I, Anderova M, Chvatal A. Quantification of astrocyte volume changes during ischemia in situ reveals two populations of astrocytes in the cortex of GFAP/EGFP mice. J Neurosci Res 2009; 87: 96–111.

17 Oberheim NA, Takano T, Han X, He W, Lin JH, Wang F et al. Uniquely hominid features of adult human astrocytes. J Neurosci 2009; 29: 3276–3287.

18 McCarty DM. Self-complementary AAV vectors; advances and applications. Mol Ther 2008; 16: 1648–1656.

19 McCarty DM, Monahan PE, Samulski RJ. Self-complementary recombinant adeno-associated virus (scAAV) vectors promote efficient transduction independently of DNA synthesis. Gene Therapy 2001; 8: 1248–1254.

20 McCarty DM, Fu H, Monahan PE, Toulson CE, Naik P, Samulski RJ. Adeno-associated virus terminal repeat (TR) mutant generates self-complementary vectors to overcome the rate-limiting step to transduction in vivo. Gene Therapy 2003; 10: 2112–2118.

21 Wang Z, Ma HI, Li J, Sun L, Zhang J, Xiao X. Rapid and highly efficient transduction by double-stranded adeno-associated virus vectors in vitro and in vivo. Gene Therapy 2003; 10: 2105–2111.

22 Nathwani AC, Gray JT, Ng CY, Zhou J, Spence Y, Waddington SN et al. Self-complementary adeno-associated virus vectors containing a novel liver-specific human factor IX expression cassette enable highly efficient transduction of murine and nonhuman primate liver. Blood 2006; 107: 2653–2661.

23 Fontana A, Fierz W, Wekerle H. Astrocytes present myelin basic protein to encephalitogenic T-cell lines. Nature 1984; 307: 273–276.

24 Samaranch L, San Sebastian W, Kells AP, Salegio EA, Heller G, Bringas JR et al. AAV9-mediated expression of a non-self protein in nonhuman primate central nervous system triggers widespread neuroinflammation driven by antigen-presenting cell transduction. Mol Ther 2014; 22: 329–337.

25 Hollak CE, Wijburg FA. Treatment of lysosomal storage disorders: successes and challenges. J Inherit Metab Dis 2014; 37: 587–598.

26 Sands MS, Davidson BL. Gene therapy for lysosomal storage diseases. Mol Ther 2006; 13: 839–849.

27 Xia H, Mao Q, Eliason SL, Harper SQ, Martins IH, Orr HT et al. RNAi suppresses polyglutamine-induced neurodegeneration in a model of spinocerebellar ataxia. Nat Med 2004; 10: 816–820.

28 Costa Mdo C, Luna-Cancalon K, Fischer S, Ashraf NS, Ouyang M, Dharia RM et al. Toward RNAi therapy for the polyglutamine disease Machado-Joseph disease. Mol Ther 2013; 21: 1898–1908.